Journal of Environmental Chemical Engineering 9 (2021) 106577

Contents lists available at ScienceDirect

Journal of Environmental Chemical Engineering

journal homepage: www.elsevier.com/locate/jece

Designed organomicaceous materials for efficient adsorption of iodine

Francisco J. Osuna [a], Esperanza Pavón [a,b], M. Carolina Pazos [c], María D. Alba [a,*]

[a] Instituto Ciencia de Materiales de Sevilla (CSIC-US), Avda. Américo Vespucio, 49, 41092 Sevilla, Spain
[b] Departamento de Física de la Materia Condensada, Universidad de Sevilla, Avda. Reina Mercedes, s/n, 41012 Sevilla, Spain
[c] Escuela de Ciencias Químicas, Universidad Pedagógica y Tecnológica de Colombia UPTC, Avda. Central del Norte, Vía Paipa, Tunja, 39-115 Boyacá, Colombia

ARTICLE INFO

Editor: V. Victor

Keywords:
Iodine capture
Synthetic mica
Adsorption
Organomica
Anionic radionuclide

ABSTRACT

The anionic iodine ^{129}I has a significant contribution to overall long-term dose resulting from the nuclear waste storage and its immobilization by clay barrier is crucial. Organoclays have been tested as ideal adsorption materials, being the clay layer charge and the length and type of organic molecules the most relevant parameters affecting the adsorption. In this work, a family of designed organomicas are explored in term of iodine adsorption capacity. Their adsorption capacities were always higher than that of the traditional clays and organoclays. C_{18}-M4 shows a maximum monolayer adsorption capacity one order of magnitude higher than natural organoclays, with a free energy typical of physical adsorption and adsorption sites of high affinity. However, its surface is not homogeneous in terms of stability constant according to the Scatchard adsorption parameters. Hence, this study can provide a guidance for the design and construction of ultrahigh-capacity iodine adsorbents.

1. Introduction

With the rapidly growing needs of current worldwide energy and the increasingly serious global warming, nuclear energy is becoming one of the most prominent and feasible alternative sources to minimize greenhouse gas emissions. Among long life elements, only ^{129}I, ^{36}Cl and ^{79}Se are able to migrate significantly from a nuclear repository [1]. Iodine ^{129}I will make a significant contribution to potential overall long-term dose resulting from the waste storage [1,2]. Indeed, it is frequently the limiting radionuclide in the performance assessment of nuclear waste disposal landfills because it forms water-soluble species such as iodide and iodate [3]. Therefore, it is urgent to find effective means to capture and store volatile radionuclide iodine for public and nuclear safety because is a higher risk to groundwater contamination [4].

Iodine can be found in a variety of oxidation states [5]. Among them, the iodide anion (I^-) is the soluble specie found in clayey formations characterized by a near-neutral pH and low redox potential [6–8]. Thus, anionic pollutants such as I^- are challenging to deal because the majority of natural minerals are either neutral or have a negative net charge [9]. And to efficiently remove them from aqueous systems, cationic framework materials that exhibit strong targeted host–guest interaction should be highly desirable [10–13].

Moreover, bentonites have been commonly proposed as host or backfill materials in the design of spent nuclear fuel and fission products repositories, HLRW [14]. Although most of the clay minerals exhibit excellent retention capabilities for cationic radionuclides, they exhibit weak interaction with anions due to their negative layer charge [15].

However, their anionic adsorption capacity can be substantially improved if the inorganic interlayer cations of clay minerals are exchanged by organic ones, forming organoclays [4,16]. In fact, the anionic adsorption capacity of organoclay was compared with other minerals (hydroxides, oxides, sulfides, silicates and organic matter) [17] and organic matter [18–20] revealing that organoclays are the most promising candidate materials for the iodide retention in HLRW repositories [17]. Even more, in the contaminated water systems, anions with higher charge densities tan iodine (i.e. NO_3^-, SO_4^{2-}, PO_4^{3-} or SiO_3^{2-}) often coexist in huge excess. Consequently, there are various challenges to be afford such as low adsorption efficiency and selectivity [21]. Sheng et al. [11] have reported a strategy for building specific types of cationic adsorbents for a selective anionic radionuclide that consists on building a hydrophobic cationic cavity that can efficiently recognize the low-charge anion through hydrophobic hydrogen bond interactions.

The organo-functionalization of a new family of swelling high charged micas, Na-M*n* ($n = 2$ or 4, layer charge), has attracted much interest in the adsorption of cationic and neutral contaminant but they have not been tested for anionic contaminants yet [22,23]. Those synthetic micas have a charge density similar to brittle micas but with a higher swelling capacity, higher crystallinity and controllable

* Corresponding author.
E-mail address: alba@icmse.csic.es (M.D. Alba).

https://doi.org/10.1016/j.jece.2021.106577
Received 9 June 2021; Received in revised form 19 August 2021; Accepted 10 October 2021
Available online 13 October 2021
2213-3437/© 2021 The Author(s). Published by Elsevier Ltd. This is an open access article under the CC BY-NC-ND license (http://creativecommons.org/licenses/by-nc-nd/4.0/).

composition [24–26]. In this way, those synthetic micas overcome some limitations, such as colloidal stability [27] and adsorption capacity [28, 29], of the natural clay minerals to be used as adsorbents.

Thus, the objectives of this work are: 1) quantify the iodine adsorption capacity of a set of as-made and organofunctionalized synthetic micas in comparison with a natural bentonite of reference; and; 2) a thermodynamical study of the iodine adsorption in the organomica with the best adsorption capacity.

2. Experimental

2.1. Materials

Synthetic swelling high-charge micas, Na-M*n* (layer charge, $n = 2$ and 4), with hydrated Na^+ in the interlayer space and these micas functionalized with molecules of dodecylammonium, C_{12}, and octadecylammonium, C_{18}, (C_{12}-M*n* and C_{18}-M*n*, respectively) from the primary amines (CAS no. 124-22-1, ≥ 99.5% purity and CAS no. 124-30-1, ≥99% purity) were synthetized following the methods described by Alba et al. [20] and Pazos et al. [17], respectively.

As a reference, Febex bentonite, supplied by the Spanish national nuclear management company, ENRESA, has been used as-received and after its functionalization was carried out with octadecylammonium molecules (C_{18}-Febex) [23].

2.2. Adsorption experiments

Batch adsorption experiments have been carried out in the following way: 0.25 g of adsorbents was mixed with 25 mL of a KI (CAS no. 7681-11-0, ≥ 99% purity) solution with a concentration of 30 meq/L. The system was allowed to equilibrate at 25 ºC for 24 h with continuous stirring at 50 rpm. Subsequently, the solid and liquid phases were separated by centrifugation at 10,000 rpm at 8 °C for 25 min.

For the adsorption isotherm at room temperature (RT), 0.25 g of C_{18}-M4 were dispersed with 25 mL of a KI solution at different concentrations (0.07–30 meq/L, see Table S1). The systems were allowed to equilibrate for 24 h under continuous stirring at 50 rpm. Subsequently, the solid and liquid phases were separated by centrifugation at 10,000 rpm at 8 °C for 25 min.

To ensure the stability of the iodine species in the initial solutions and after adsorption, the pH and electromotive force (E_h) were measured. These values have been plotted in the Iodine Pourbaix diagram (Fig. S1), showing that the anion I^- was always the stable specie in such conditions.

Finally, the initial solutions and those obtained after adsorption (after filtering to remove the residual solid if needed) were kept in a glass bottle in the freezer prior to their characterization.

2.3. Characterization

Electromotive force (E_h) and pH values of the initial solutions and supernatants were measured at room temperature using a Eutech Instruments PC 700 pH-meter.

The iodine analysis was carried out by inductively coupled plasma-mass spectrometry (ICP-MS); the difference of iodine concentration before (C_i) and after sorption (C_{eq}) reveals the amount of adsorbed iodine (C_s, mg/kg) [30]:

$$C_s = (C_i - C_{eq}) \cdot \frac{V}{m}$$

where the V (L) is the volume of the solution, m is the weight of the mica (kg), C_i (mg/L) and C_{eq} (mg/L) are the concentration of the iodine in initial and final solutions, respectively.

The adsorption percentage and the distribution ratio (K_d, L/kg), were calculated as follows [30]:

$$\%\ \ ads. = \frac{C_i - C_{eq}}{C_i} \cdot 100$$

$$K_d = \frac{C_s}{C_{eq}}$$

Three mathematical models have been used for the isotherm analysis: Freundlich, Langmuir and Scatchard isotherm models.

The Freundlich adsorption isotherm is one of the most widely used mathematical descriptions of multilayer adsorption on a heterogeneous adsorbent surface [31]. This isotherm gives an expression encompassing the surface heterogeneity and the exponential distribution of active sites and their energy. It can be written as follows [32]:

$$C_s = K_F \cdot C_{eq}^{\ n_F}$$

K_F (L/kg) is the Freundlich constant, which is related to adsorption capacity, and n_F (dimensionless) is the adsorption intensity. If n_F value is above 1, this implies that sorption process is chemical, but if n_F value is below 1, sorption is favorable for a physical process [33,34]. Values of $0.1 \leq n_F \leq 0.45$ means that sorption was favorable and highly non-linear [35].

Langmuir equation shows the monolayer adsorption effect of the adsorbent and assumes that adsorption takes place at specific sites on the surface [31]. It is based on the fact that the attraction between molecules decreases when they move away from the surface. This model is defined with the formula [31]:

$$C_S = \frac{Q_{max} \cdot K \cdot C_{eq}}{K \cdot C_{eq} + 1}$$

where Q_{max} (mg/kg) is the maximum adsorbed concentration corresponding to complete monolayer coverage and K (L/mg) is an equilibrium constant related to the adsorption energy.

The essential characteristics of the Langmuir isotherm can be expressed by the parameter R_L (dimensionless) related to the equilibrium parameter as follow [34]:

$$R_L = \frac{1}{1 + K \cdot C_{imax}}$$

where C_{imax} (mg/L) is the maximum initial concentration. Adsorption is unfavorable if $R_L > 1$, it is linear if $R_L = 1$, favorable when $0 < R_L < 1$ and irreversible if $R_L = 0$ [34].

From K, the thermodynamic parameters of adsorption can be evaluated [35]:

$$\Delta G^o = -R \cdot T ln K$$

where, R is the ideal gas constant ($8.314 \cdot 10^{-3}$ kJ/mol·K), T is the temperature (298 K) and K is the equilibrium constant of the Langmuir equation in L/mol.

Finally, Scatchard adsorption plot analysis is useful to determine whether adsorption occurs at a single type of site or at several when C_s/C_{eq} vs C_s is plotted [34]:

$$\frac{C_s}{C_{eq}} = K_s n_s - K_s C_s$$

The Scatchard plot gives a measure of the fraction of adsorbate retained on the solid at different adsorbate concentrations. A break in the slope of the curve indicates an inhomogeneous surface in terms of stability constant [36]. A higher constant K_s (L/mg) indicates a more active site. The constant n_s is the number of adsorption sites but must be interpreted qualitatively. The main interest is to identify the type of sites and the nature of the type of adsorption [37].

Thermogravimetric analysis, TG, were carried out using a TA (model STD-Q600) instrument, in Characterization Service (CITIUS, University of Seville, Spain), with alumina as reference. The temperature was increased at a constant rate of 10 °C/min. The temperature of each loss

weight on the TG was determined thorough the derivative TG curve as a function of temperature (DTG).

X-ray diffraction (XRD) patterns were obtained at the CITIUS X-ray laboratory (University of Seville, Spain) on a Bruker D8 Advance instrument equipped with a Cu K_α radiation source operating at 40 kV and 40 mA. Diffractograms were obtained in the 2θ range of 3–70° with a step size of 0.015° and a step time of 0.1 s.

The binding energy of the iodine was analyzed using X-ray photoelectron spectroscopy at the XPS Service (SCAI, University of Cordoba, Spain). The XPS spectrometer SPECS mod. PHOIBOS 150 MCD is equipped with a twin anode (Mg and Al) monochromatized X-ray source. All scans given in this work were obtained with the Mg source and binding energies were reference to C (1s) signal at 284.8 eV.

The morphology and elemental composition of the crystalline phases after the treatments were analyzed by scanning electron microscopy (SEM/EDX), using a JEOL microscope (JSM 5400 Model) and working at 20 kV, which is installed in the Microscopy Service of ICMS (CSIC-US). This equipment is connected to an energy dispersive X-ray system (EDX) (Oxford Link ISIS) which allows chemical analysis of samples using a detector of Si/Li with a Be window.

3. Results and discussion

3.1. Influence of the framework and interlayer space of swelling high charge mica on iodine adsorption

Iodine adsorption percentage and derived K_d constant for each adsorbent system are shown in Table 1, together with the values found in the literature for similar adsorption systems. Within the same experimental conditions, iodine adsorption is negligible in raw Febex bentonite, whereas it is present in the synthetic samples. In these last, the percentage of adsorption is an order of magnitude higher in Na-M4 than in Na-M2. These results are improved by the clay organo-functionalization, which increases considerably the amount of adsorbed iodine in all samples, particularly in C_{18}-Febex.

Water content in clays before adsorption was calculated from the weight loss data in the region between 25 ºC and 150 ºC. Fig. 1a shows the correlation between adsorption capacity and water content. A drop in the adsorption capacity (C_s and % ads.) is observed when the water content increases due to the hydrophilic environment of the interlayer space that inhibits the iodine adsorption.

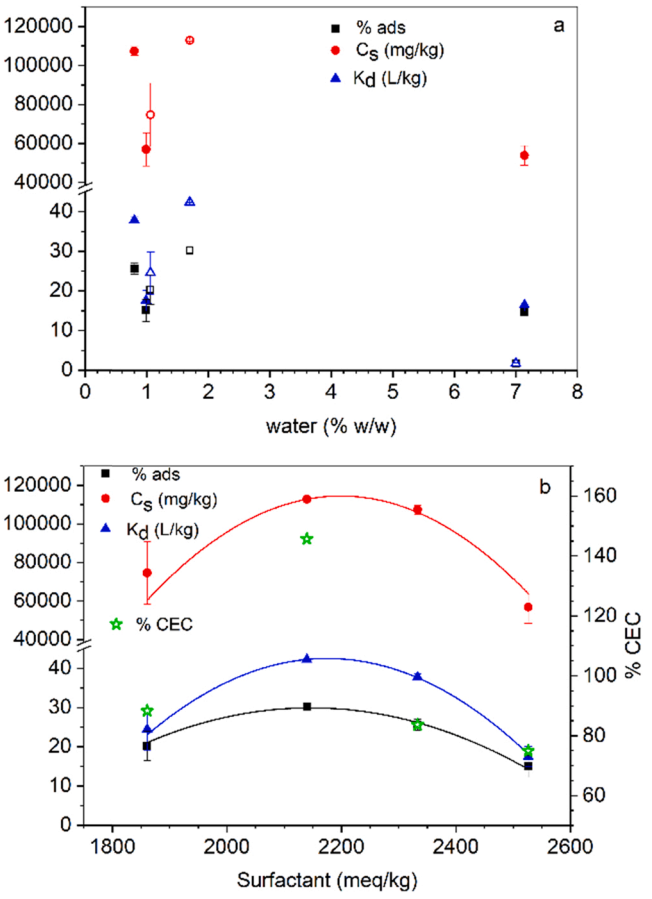

Fig. 1. Iodine adsorption capacity and % CEC of surfactant as a function of: a) water content; and; b) surfactant content.

Regarding the adsorption of iodine in organoclays, the adsorption increases when the length of the alkyl chain also increases: C_{18}-M*n* > C_{12}-M*n* > Na-M*n*. Bors et al. [38] observed that the anion adsorption capacity by organobentonites depends on the organophylicity of the adsorbent system, and hence, the nature of the organic

Table 1
Adsorption parameters of synthetic micas, natural clay minerals, active carbon and viscogel.

Sorbent		Adsorption conditions			Adsorption parameters		Ref.
sample	%CEC surf[a]	C_i (meq/L)	L/S[b] (mL/g)	t (days)	% ads	K_d (L/kg)	
Na-M2	0	30	100	1	1.7 ± 0.2	1.7 ± 0.2	This work
Na-M4	0				14.7 ± 0.8	16.5 ± 1.5	
Febex	0				0.2 ± 0.2	0.3 ± 0.2	
C_{12}-M2	90				20.3 ± 3.7	24.6 ± 5.3	
C_{18}-M2	125				30.2 ± 0.9	42.3 ± 0.1	
C_{12}-M4	85				15.1 ± 2.8	17.6 ± 2.6	
C_{18}-M4	95				25.7 ± 1.4	37.8 ± 0.8	
C_{18}-Febex	130				17.2 ± 3.5	20.8 ± 3.2	
HDPy-MX80	150	1000	5	28	–	400.0	[42]
C_{16}-MX80	200	10	20	21	1.5	–	[43]
HDTMA-MX80	200				50.0	–	
HDPy-MX80	200				60.0	–	
Active carbon	–	10	100	2	15.0	18.0	[17]
HDPy-MX80	–				30.0	42.0	
Hydrotalcite	–				14.0	16.0	
HDPy-Bentonite	–		–	–	33.0	49.0	
Viscogel B4	–				17.0	21.0	
Bentonite: HDPy-Bentonite (4:1)	20	4	100	2	0	0	[40]
Bentonite: HDPy-Bentonite (1:1)	50				3.3	3.5	
Bentonite: HDPy-Bentonite (0:1)	100				24.4	30.0	

[a] % CEC satisfied by the surfactant.
[b] KI solution volume/sorbent mass.

agents may play an important role. This fact is corroborated with our results: clays organophylicty increases with the alkyl chain [39] as well as iodine adsorption does. Moreover, the dependence of iodine adsorption on the nature of clays has already been observed by Dultz and Bors [16], who compared the adsorption of MX80 with the adsorption of vermiculites. In this research when all clays are organofunctionalized with octadecylammonium, the adsorption capacity of synthetic micas is higher than Febex bentonite and quite similar between both micas: C_{18}-M2 $\geq$ C_{18}-M4 $>>$ C_{18}-Febex.

Rao and Sivachidambaram [40] detected two iodine adsorption mechanisms in organoclays. Firstly, iodine is adsorbed by coulombic interactions to the cationic head groups and the alkyl chain of the surfactant (primary adsorption sites). Secondly, it is adsorbed by ion exchange reaction with Cl^- together with excess alkylammonium molecules that form ionic pairs with Cl^- (secondary adsorption sites). Dultz and Bors [16] observed that ionic force are effective at lower alkylammonium ions, $HDPy^+$, loading, and van der Waals forces operate when alkylammonium ions are taken up in excess of the cation exchange capacity (CEC) and the existence of HDPyBr ion pair being assumed. Therefore, iodine adsorption increases when the amount of surfactant exceeds the CEC of the clay minerals because both adsorption mechanisms are operative.

The adsorption parameters (C_s, % ads. and K_d) have been represented as a function of the amount of surfactant loading (S, meq/kg), Fig. 1b, with a non-linear variation observed. The plots can be fitted using polynomial equations and the statistical parameters of the fit are summarized in Table S2:

$$\%ads. = -470.017 + 0.466 \cdot S - 1.085 \cdot 10^{-4} \cdot S^2$$

$$C_s = -2.167 \cdot 10^6 + 2077.50 \cdot S - 0.4724 \cdot S^2$$

$$K_d = -891.137 + 0.8586 \cdot S - 1.947 \cdot 10^{-4} \cdot S^2$$

Below the CEC, a linear increase is observed with the amount of CEC satisfied, which is due to an increase in organophilia [41,42] and a maximum adsorption is obtained at ca. 145% CEC. Thus, the CEC satisfied by the surfactant is the key factor for the adsorption efficiency but not the absolute surfactant amount.

Table 1 shows a comparison of the adsorption capacity obtained in this research with the values found for micas and other adsorbents. As far as we know, there is only one study carried out with a natural clay without organofunctionalization. It is the hydrotalcite case, a layered silicate with positive charged surface. Comparing our results, the iodine adsorption of Na-M4 was similar than hydrotalcite, despite mica is not the ideal target for an anionic adsorption. Active carbon, a very promising adsorption agent [17], is also compared, leaving the same adsorption capacity than Na-M4, viscogel B4 and hydrotalcite and the adsorption capacity of organomicas is higher (Table 1). More examples for iodine adsorption can be found in organoclays. Alkylamonium ions have been tested in MX80 bentonite, particularly C_{16}. C_{12}-M*n* and C_{18}-M*n* show an adsorption percentage one order of magnitude higher than C_{16}-MX80, although the contact time was considerable shorter (1 days vs 21 day, respectively) [43]. However, when other organic molecules are used for the organofunctionalization, a different behavior is observed. The adsorption capacity of C_{12}-M*n* and C_{18}-M*n* is slightly lower than MX80 bentonite functionalized with hexadecyltrimethylammonium (HDTMA-MX80) and with hexadecylpyridine (HDPy-MX80) [43], but two factors must be taken into account that influence this behavior:

- Lower initial concentrations, ten times longer contact times and higher % CEC satisfied by surfactant in MX80 [43].
- Alkyltrimethylammonium and alkylpyridine confer a more organophilic character than alkyl ammonium chains, which favors the adsorption of anions [38].

The adsorption sites of iodine have been analyzed by XPS in the region of I $3d_{5/2}$ signal (Fig. S2) and the fit parameters of the X-M*n* peaks have been analyzed, Table 2. In all the samples, the main signal appears at ca. 619 eV which is characteristic of I^- combined with alkali metals and, thus, may be due to I^- adsorbed in the interlayer space as ionic pair with Na^+, K^+ or R-NH_3^+ [44]. Additionally, a second minority signal (10% of the total signal) appears at a binding energy of ca. 620 eV in the organomicas. This additional signal has been described as I^- associated with methyl groups [45] and could be due to iodides adsorbed on the alkyl chain of the surfactant.

KI adsorption in Na-M*n* provokes a slight increase in the basal spacing, as shown by XRD analysis (Fig. 2) whereas the adsorption in Febex produces a minor decrease in this distance (Fig. S3). This is mainly due to the cation exchange reaction that is produced during the adsorption. Na^+ and Na^+/Ca^{2+} are the interlayer cations in Na-M*n* and Febex, respectively. In the adsorption process, hydrated Na^+ ions are replaced by hydrated K^+, and consequently, in Na-M*n*, a higher basal space is observed in XRD due to the higher K^+ hydration capacity compared to Na^+ [46]. In Febex there is no change in the basal space because it is governed by the higher hydration capacity of Ca^{2+} [46].

No change in the basal distance in organoclays is observed (Fig. 2), due to their large interlayer space (4.90 and 3.6 nm for C_{18}-M*n* and C_{12}-M*n*, respectively), that does not change when iodine is adsorbed.

The SEM imagines (Figs. S4 and S5) reveal that the adsorption process does not modify the laminar morphology of the clays. However, the EDX spectra of the raw bentonite, Fig. S4a, and Na-M*n*, Fig. 3a, before and after adsorption reveals changes in the chemical composition of the layers. The Na K_α line decreases and the K K_α line appears due to the exchange of Na^+ by K^+, as observed by XRD. In the case of organoclays, the I L_α line is observed and the intensity of this line is in good agreement with the ICP-MS data. In addition, the K K_α line is observed in the organoclays, which agrees with the XPS data that confirm the presence of iodine adsorbed as an ionic pair of K^+.

3.2. Adsorption isotherm of C_{18}-M4

As observed above, Na-M4 showed a higher adsorption capacity than Na-M2, and Mica-4 functionalized with octadeylammonium (C_{18}-M4) was a better adsorbent than the as-made one (Na-M4) and it functionalized with dodecylammonium (C_{12}-M4). Therefore, the adsorption isotherm experiment was carried out in C_{18}-M4.

Adsorption isotherm is an important analysis when characterizing clays chemical retention. Giles et al. [47] classified adsorption isotherms based on their initial slopes and curvatures. However, the best way to identify the isotherm class and subgroup is to plot i) the distribution coefficient (K_d) vs. the amount of solute adsorbed into the solid phase (C_s), and, ii) log K_d vs log C_s. C_{18}-M4 KI adsorption isotherm, Fig. 4a, matches L-type with a plateau, even though the adsorption limit has not been completely reached [48]. However, the plot of K_d vs C_s and logK_d vs logC_s, Fig. 4b and c respectively, indicates a S2-type isotherm [47]. This type of isotherm has two causes. Firstly, solute–solute attractive forces at the surface cause cooperative adsorption which leads to the S-shape [47]. Secondly, the sorption of a solute may be inhibited by a competing reaction within the solution, such as a complexation reaction with a

Table 2
XPS I $3d_{5/2}$ peaks analysis.

Sample	Region I (CH_3I)		Region II (I^-)	
	BE (eV)	%	BE (eV)	%
Na-M2	–	–	619.1	100
C_{12}-M2	620.7	16.2	618.6	83.8
C_{18}-M2	620.8	8.3	618.7	91.7
Na-M4	–	–	619.2	100
C_{12}-M4	620.3	12.5	618.2	87.6
C_{18}-M4	620.3	11.7	618.2	88.3

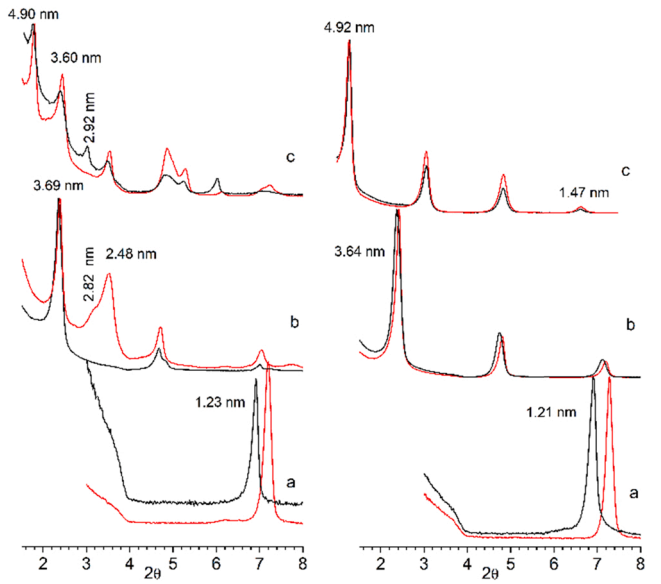

Fig. 2. XRD patterns of X-M*n* ($n = 2$, left, and $n = 4$, right) before (red line) and after KI adsorption (black line): a) Na-M*n*; b) C_{12}-M*n*: and; c) C_{18}-M*n*. (For interpretation of the references to color in this figure legend, the reader is referred to the web version of this article.)

ligand [47]. The S-class isotherm occurs less frequently but is usually observed in the adsorption of surfactants [47].

The evolution of the partition constant, K_d, with the amount of iodine adsorbed and with the initial iodine concentration (Fig. 4b) consists of two segments:

- At initial concentration below ca. 50 ppm ($C_s \leq 5000$ mg/kg), K_d increases with concentration, with the maximum value at an initial concentration of 50 ppm (C_{18}-M4-C).
- At initial concentration above ca. 50 ppm ($C_s > 5000$ mg/kg), K_d decreases exponentially as the amount of iodine adsorbed increases, indicating adsorption predominantly at non-specific sites [49].

This evolution indicates that at low concentrations, iodine is first adsorbed at specific sites and, once saturated begins to prevail adsorption at non-specific sites.

The adsorption isotherm, Fig. 4a, exhibits a maximum adsorption value of ca. $1.10 \cdot 10^5$ mg/kg = 1587.7 meq/kg that is below the amount of octadecylammonium adsorbed, 2088.9 meq/kg. The isotherm has been adjusted to three different mathematical models and fit parameters are shown in Table 3 and the statistical parameters of the fits in Table S3.

Using Freundlich model, the experimental data were fitted to a single adsorption site whose K_F is high and indicating that the sites are of high affinity [50]. Moreover, n_F value is between 0.1 and 0.5 indicating a good adsorption capacity. These data are compared with those obtained from isotherms in natural clays [37,40], Table 3. It is observed that C_{18}-M4 exhibits a higher K_F value than natural montmorillonites and those modified with long chain polymers and, consequently, C_{18}-M4 has a higher iodine adsorption affinity [37]. Moreover, its K_F is higher than K_F of bentonites modified with hexadecylpyridinium cations, HDPy-bentonite. This is a remarkable fact because HDPy confers a more organofilic character to bentonite than alkylammonium does to mica and consequently, a higher anion adsorption capacity should be expected in HDPy-bentonite [38].

The maximum adsorption capacity of the monolayer, Q_{max}, obtained by the Langmuir adjustment, is also an order of magnitude higher than that of HDPy-bentonite [40]; its equilibrium constant was associated with adsorption energy is lower.

The equilibrium parameter R_L shows that the adsorption in C_{18}-M4 is favorable as corroborated by the free energy value, calculated from K, of −14.88 kJ/mol, consistent with an electrostatic interaction and physical adsorption [51].

Finally, the Scatchard fit shows a break in the slope of the curve, indicating an inhomogeneous surface in terms of stability constant. The strongest adsorption (Site I) is due to iodine adsorption on the hydrophobic part of the octadecylammonium chain and adsorbate-adsorbate adsorption and the weaker adsorption (Site II) could be due to adsorption in the hydrophilic part [37].

Krishna et al. [37] observed up to three iodine adsorption sites have been observed in organoclays:

- Site I: in the oleic chain
- Site II: in the ethylene oxide groups
- Site III: adsorbate-adsorbate interaction, which occurs when the surface is saturated.

Being $K_s(III) > K_s(I) > K_s(II)$.

The evolution of the interlayer spacing has been followed by XRD, Fig. 5, and no change is observed in this distance because the gallery size in C_{18}-M4 is large enough to accommodate iodine ions without disrupting the interlayer space. However, XRD diagrams from higher initial concentrations samples exhibit reflections due to KI at high angles (marked with asterisks).

The analysis of the EDX spectra before and after adsorption has

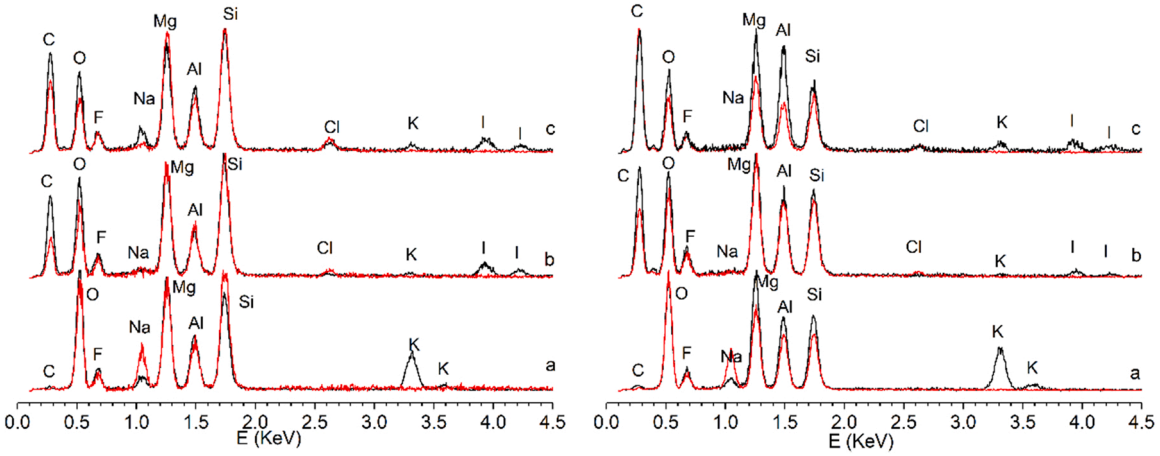

Fig. 3. EDX spectra of X-M*n* ($n = 2$, left, and $n = 4$, right) before (red line) and after KI adsorption (black line): a) Na-M*n*; b) C_{12}-M*n*: and; c) C_{18}-M*n*. (For interpretation of the references to color in this figure legend, the reader is referred to the web version of this article.)

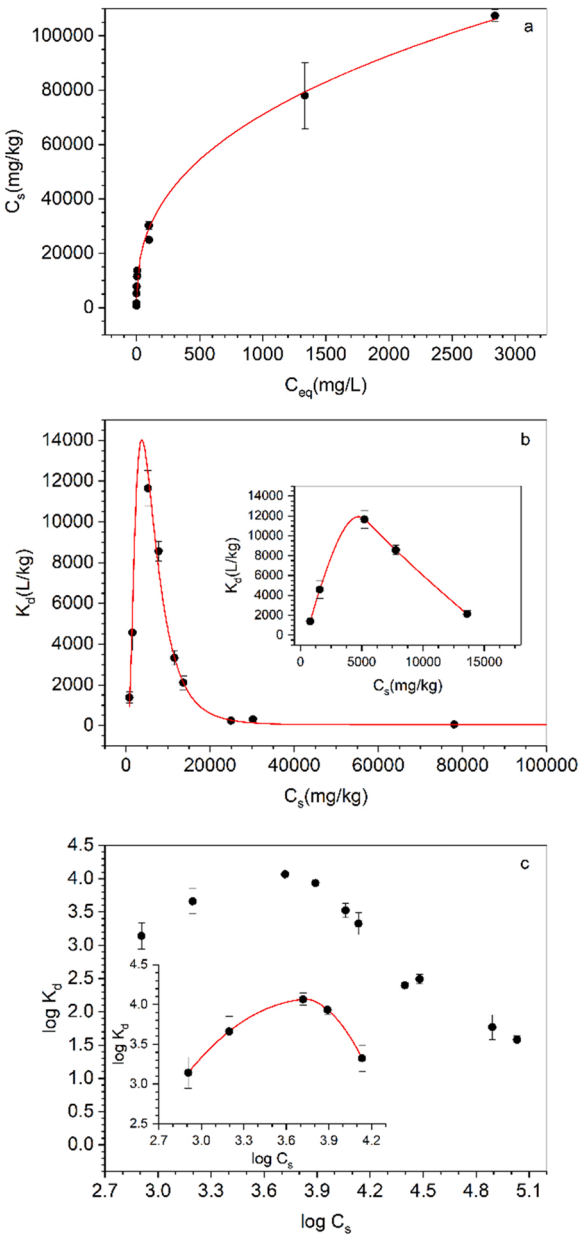

Fig. 4. Iodine adsorption isotherm of C_{18}-M4.

allowed obtaining the ratio between interlayer cations and anions and magnesium in the framework, Fig. 6. The amount of adsorbed iodine (I/Mg ratio), Fig. 6a, increases with increasing initial concentration (C_{18}-M4-A vs C_{18}-M4-K). At the lowest initial concentration (C_{18}-M4-A), the amount of Cl^- (Cl/Mg ratio) remains constant. As previously reported, the K_d value was high due to iodine associated with the alkylammonium chain. At the maximum initial concentration (C_{18}-M4-K), the Cl^- (Cl/Mg ratio) decreases almost by half, inferring that there is also an ionic exchange between I^- and Cl^- compatible with a drop in K_d values (Fig. 4).

At the highest initial concentration, an increase of (Na+K/Mg ratio), Fig. 6b, is observed and is compatible with the appearance of the KI reflections in the XRD pattern (Fig. 5).

4. Conclusions

Synthetic micas are good adsorbents for iodide anions, increasing their adsorption capacity when functionalized with alkylammonium cations. Their adsorption capacity was always higher than that of previous natural clays.

In organomicas, iodine adsorption increases as the length of the alkyl chain does: C_{18}-M*n* > C_{12}-M*n* > Na-M*n*. When micas are organo-functionalized with octadecylammonium, the iodine adsorption capacity is independently of the mica layer charge.

In sodium micas, a cationic exchange of Na^+ by K^+ occurs, leaving the adsorbed iodide as a counterion of Na^+ and/or K^+. In organomicas, a part of the adsorbed iodide is associated with the remaining K^+ and/or Na^+ and other part is associated with the alkyl chain of the surfactant.

The KI adsorption isotherm on C_{18}-M4 shows that the adsorption sites are of high affinity and this organomica exhibits a good adsorption capacity. Furthermore, its maximum monolayer adsorption capacity,

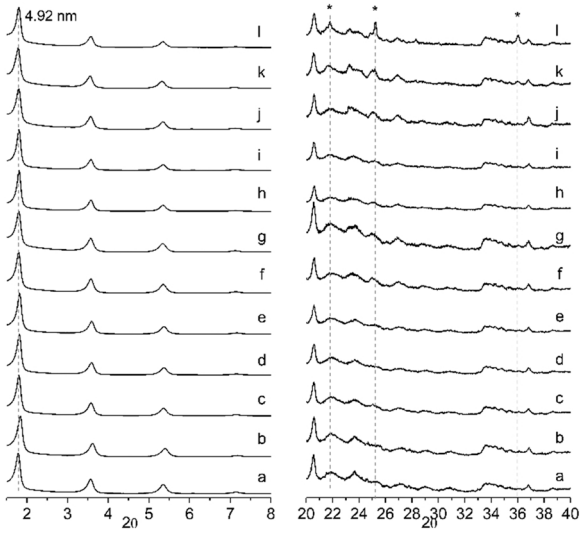

Fig. 5. XRD patterns of C_{18}-M4 before (a) and after (b–l; from C_{18}-M4-A to C_{18}-M4-K, see Table S1) KI adsorption. *=KI (PDF 00-01-554).

Table 3
Fit parameters of the C_{18}-M4 iodine adsorption isotherm compared with the data previously obtained in other natural clay minerals.

Conditions	Sorbents	Fit Parameters			Ref.
		Freundlich	Langmuir	Scatchard	
RT, 24 h	C_{18}-M4	$K_F = 6.21{\cdot}10^3$ L/kg $n_F = 0.33$	$K = 3.15{\cdot}10^{-3}$ L/mg $Q_{max} = 1.10{\cdot}10^5$ mg/kg $R_L = 0.08$	K_s (I) = 1.05 L/mg n_s (I) = $1.56{\cdot}10^4$ mg/kg K_s (II) = $2.47{\cdot}10^{-3}$ L/mg n_s (II) = $1.22{\cdot}10^5$ mg/kg	This work
RT, 48 h	HDPy-Bentonite	$K_F = 2.61{\cdot}10^3$ L/kg $n_F = 0.23$	$K = 2.97{\cdot}10^{-2}$ L/mg $Q_{max} = 1.44{\cdot}10^4$ mg/kg $R_L = 0.03$		[40]
RT, 0.5 h	Mont	$K_F = 1.38{\cdot}10^{-3}$ L/kg $n_F = 0.34$		K_s (I) = $2.7{\cdot}10^{-3}$ L/mg n_s (I) = $2.34{\cdot}10^4$ mg/kg K_s (II) = $5.3{\cdot}10^{-4}$ L/mg n_s (II) = $5.61{\cdot}10^4$ mg/kg	[37]
	TWEE80-Mont	$K_F = 5.80{\cdot}10^{-3}$ L/kg $n_F = 0.75$		K_s (I) = $1.1{\cdot}10^{-3}$ L/mg n_s (I) = $6.53{\cdot}10^5$ mg/kg K_s (II) = $3.3{\cdot}10^{-4}$ L/mg n_s (II) = $1.14{\cdot}10^6$ mg/kg	
	PEG300-Mont	$K_F = 4.56{\cdot}10^{-3}$ L/kg $n_F = 0.20$		$K_s = 2.2{\cdot}10^{-4}$ L/mg $n_s = 2.78{\cdot}10^5$ mg/kg	

Mont=montmorillonite.

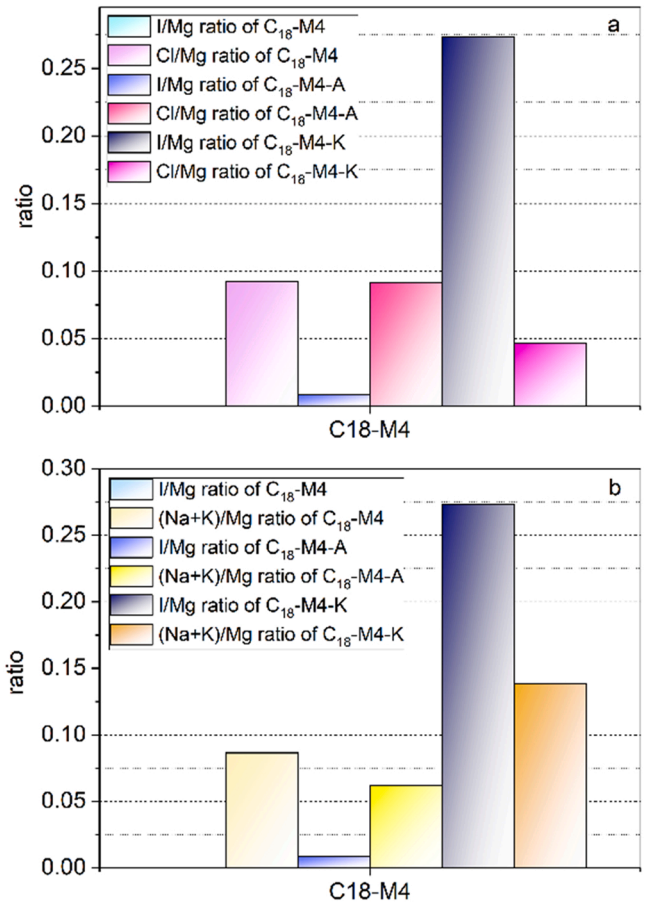

Fig. 6. Relative intensity of EDX signals of C_{18}-M4 after KI adsorption for the lowest and highest initial concentration of the isotherm (see Table S1).

Q_{max}, is an order of magnitude higher than that of HDPy-bentonite, with a free energy typical of physical adsorption. However, its surface is not homogeneous in terms of stability constant. There is a stronger adsorption site (Site I) due to adsorption in the hydrophobic part of the octadecylammonium chain and adsorbate-adsorbate adsorption and a weaker adsorption (Site II) due to adsorption in the hydrophilic part, in agreement with the EDX spectra.

Declaration of Competing Interest

The authors declare that they have no known competing financial interests or personal relationships that could have appeared to influence the work reported in this paper.

Acknowledgment

We would like to thank ENRESA (contract nº 0079000237) for financial support. Dr. Pavón thanks University of Seville for the financial support of her current contract from VI PPIT-US program.

Appendix A. Supporting information

Supplementary data associated with this article can be found in the online version at doi:10.1016/j.jece.2021.106577.

References

[1] S. Altmann, 'Geo'chemical research: a key building block for nuclear waste disposal safety cases, J. Contam. Hydrol. 102 (2008) 174–179, https://doi.org/10.1016/j.jconhyd.2008.09.012.

[2] B. Grambow, Mobile fission and activation products in nuclear waste disposal, J. Contam. Hydrol. 102 (2008) 180–186, https://doi.org/10.1016/j.jconhyd.2008.10.006.

[3] J.G. Reynolds, J.S. Lachut, H.K. Meznarich, T.M. Ely, A.M. Templeton, G.A. Cooke, Silver-iodine association in Hanford nuclear waste, J. Radioanal. Nucl. Chem. 326 (2020) 737–741, https://doi.org/10.1007/S10967-020-07347-7.

[4] R.C. Moore, C.I. Pearce, J.W. Morad, S. Chatterjee, T.G. Levitskaia, R.M. Asmussen, A.R. Lawter, J.J. Neeway, N.P. Qafoku, M.J. Rigali, S.A. Saslow, J.E. Szecsody, P. K. Thallapally, G. Wang, V.L. Freedman, Iodine immobilization by materials through sorption and redox-driven processes: a literature review, Sci. Total Environ. 716 (2020), 132820, https://doi.org/10.1016/j.scitotenv.2019.06.166.

[5] H. Koch-Steindl, G. Pröhl, Considerations on the behaviour of long-lived radionuclides in the soil, Radiat. Environ. Biophys. 40 (2001) 93–104, https://doi.org/10.1007/s004110100098.

[6] C.A.J. Appelo, A. Vinsot, S. Mettler, S. Wechner, Obtaining the porewater composition of a clay rock by modeling the in- and out-diffusion of anions and cations from an in-situ experiment, J. Contam. Hydrol. 101 (2008) 67–76, https://doi.org/10.1016/j.jconhyd.2008.07.009.

[7] A. Vinsot, S. Mettler, S. Wechner, In situ characterization of the Callovo-Oxfordian pore water composition, Phys. Chem. Earth 33 (2008), https://doi.org/10.1016/j.pce.2008.10.048.

[8] É.C. Gaucher, P. Blanc, F. Bardot, G. Braibant, S. Buschaert, C. Crouzet, A. Gautier, J.P. Girard, E. Jacquot, A. Lassin, G. Negrel, C. Tournassat, A. Vinsot, S. Altmann, Modelling the porewater chemistry of the Callovian-Oxfordian formation at a regional scale, Comptes Rendus – Geosci. 338 (2006) 917–930, https://doi.org/10.1016/j.crte.2006.06.002.

[9] C. Tournassat, E.C. Gaucher, M. Fattahi, B. Grambow, On the mobility and potential retention of iodine in the Callovian-Oxfordian formation, Phys. Chem. Earth 32 (2007) 539–551, https://doi.org/10.1016/j.pce.2005.12.004.

[10] Y. Yang, X. Xiong, Y. Fan, Z. Lai, Z. Xu, F. Luo, Insight into volatile iodine uptake properties of covalent organic frameworks with different conjugated structures, 2019. https://doi.org/10.1016/j.jssc.2019.120979.

[11] D. Sheng, L. Zhu, X. Dai, C. Xu, P. Li, C.I. Pearce, C. Xiao, J. Chen, R. Zhou, T. Duan, O.K. Farha, Z. Chai, S. Wang, Successful decontamination of 99TcO4− in groundwater at legacy nuclear sites by a cationic metal-organic framework with hydrophobic pockets, Angew. Chem. 131 (2019) 5022–5026, https://doi.org/10.1002/ANGE.201814640.

[12] J. Li, X. Dai, L. Zhu, C. Xu, D. Zhang, M.A. Silver, P. Li, L. Chen, Y. Li, D. Zuo, H. Zhang, C. Xiao, J. Chen, J. Diwu, O.K. Farha, T.E. Albrecht-Schmitt, Z. Chai, S. Wang, TcO4− remediation by a cationic polymeric network, n.d. https://doi.org/10.1038/s41467-018-05380-5.

[13] L. Zhu, D. Sheng, C. Xu, X. Dai, M.A. Silver, J. Li, P. Li, Y. Wang, Y. Wang, L. Chen, C. Xiao, J. Chen, R. Zhou, C. Zhang, O.K. Farha, Z. Chai, T.E. Albrecht-Schmitt, S. Wang, Identifying the recognition site for selective trapping of 99TcO4− in a hydrolytically stable and radiation resistant cationic metal–organic framework, 2017. https://doi.org/10.1021/jacs.7b08632.

[14] K.A. Czurda, J.F. Wagner, Cation transport and retardation processes in view of the toxic waste deposition problem in clay rocks and clay liner encapsulation, Eng. Geol. 30 (1991) 103–113, https://doi.org/10.1016/0013-7952(91)90037-L.

[15] K.H. Lieser, T. Steinkopff, Chemistry of radioactive iodine in the hydrosphere and in the geosphere, Radiochim. Acta 46 (1989) 49–55.

[16] S. Dultz, J. Bors, Organophilic bentonites as adsorbents for radionuclides II. Chemical and mineralogical properties of HDPy-montmorillonite, Appl. Clay Sci. 16 (2000) 15–29, https://doi.org/10.1016/S0169-1317(99)00042-3.

[17] S. Kaufhold, M. Pohlmann-Lortz, R. Dohrmann, R. Nüesch, About the possible upgrade of bentonite with respect to iodide retention capacity, Appl. Clay Sci. 35 (2007) 39–46, https://doi.org/10.1016/j.clay.2006.08.001.

[18] Y. Liu, H. VonGounte, Migration chemistry and behaviour of iodide relevant to geological disposal of radioactive wastes—a literature review with a compilation of sorption data, Würenlingen, Schweiz, 1998.

[19] B. Gu, R.K. Schulz, Anion retention in soil: possible application to reduce migration of buried technetium and iodide — a review, Washington D.C., 1991.

[20] J.L. Krumhansl, P.V. Brady, P.-C. Zhang, Soil mineral backfills and radionuclide retention, in: Geochemistry of Soil Radionuclides, Soil Science Society of America, Madison, 2002.

[21] E.D. Miensah, M.M. Khan, J.Y. Chen, X.M. Zhang, P. Wang, Z.X. Zhang, Y. Jiao, Y. Liu, Y. Yang, Zeolitic imidazolate frameworks and their derived materials for sequestration of radionuclides in the environment: a review, Crit. Rev. Environ. Sci. Technol. 50 (2019) 1874–1934, https://doi.org/10.1080/10643389.2019.1686946.

[22] M.D. Alba, M.A. Castro, M.M. Orta, E. Pavón, M.C. Pazos, J.S. Valencia Rios, Formation of organo-highly charged mica, Langmuir 27 (2011).

[23] M.C. Pazos, M.A. Castro, M.M. Orta, E. Pavón, J.S.V. Rios, M.D. Alba, Synthetic high-charge organomica: Effect of the layer charge and alkyl chain length on the structure of the adsorbed surfactants, Langmuir 28 (2012) 7325–7332.

[24] T. Kodama, S. Komarneni, Na-4-mica: Cd2+, Ni2+, Co2+, Mn2+ and Zn2+ ion exchange, J. Mater. Chem. 9 (1999) 533–539.

[25] M. Park, D.H. Lee, C.L. Choi, S.S. Kim, K.S. Kim, J. Choi, Pure Na-4-mica: synthesis and characterization, Chem. Mater. 14 (2002) 2582–2589.

[26] M.D. Alba, M.A. Castro, M. Naranjo, E. Pavón, Hydrothermal reactivity of Na-n-micas (n = 2, 3, 4), Chem. Mater. 18 (2006) 2867–2872.

[27] F.J. Osuna, A. Cota, M.A. Fernández, E. Pavón, R.M. Torres Sánchez, M.D. Alba, Influence of framework and interlayer on the colloidal stability of design swelling high-charged micas, Colloids Surf. A-Physicochem. Eng. Asp. 561 (2019) 32–38, https://doi.org/10.1016/j.colsurfa.2018.09.086.

[28] F.J. Osuna, A. Cota, E. Pavón, M.C. Pazos, M.D. Alba, Cs+ immobilization by designed micaceous adsorbent under subcritical conditions, Appl. Clay Sci. 143 (2017) 293–299.
[29] F.J. Osuna, E. Pavón, M.D. Alba, Pb2+, Cd2+ and Hg2+ removal by designed functionalized swelling high-charged micas, Sci. Total Environ. 764 (2021), 142811, https://doi.org/10.1016/j.scitotenv.2020.142811.
[30] E. Galunin, M.D. Alba, M.J. Santos, T. Abrão, M. Vidal, Examination of competitive lanthanide sorption onto smectites and its significance in the management of radioactive waste, J. Hazard. Mater. 186 (2011).
[31] S. Veli, B. Alyüz, Adsorption of copper and zinc from aqueous solutions by using natural clay, J. Hazard. Mater. 149 (2007) 226–233.
[32] K.G. Bhattacharyya, S.Sen Gupta, Adsorptive accumulation of Cd(II), Co(II), Cu(II), Pb(II), and Ni(II) from water on montmorillonite: influence of acid activation, J. Colloid Interface Sci. 310 (2007) 411–424, https://doi.org/10.1016/j.jcis.2007.01.080.
[33] K.Y. Foo, B.H. Hameed, Insights into the modeling of adsorption isotherm systems, Chem. Eng. J. 156 (2010) 2–10.
[34] F.A. Dawodu, G.K. Akpomie, M.A. Abuh, Equilibrium isotherm studies on the batch sorption of copper (II) ions from aqueous solution unto “Nsu Clay”, Int. J. Sci. Eng. Res. 3 (2012) 1–7. ⟨http://www.ijser.org⟩.
[35] Ş. Kubilay, R. Gürkan, A. Savran, T. Şahan, Removal of Cu(II), Zn(II) and Co(II) ions from aqueous solutions by adsorption onto natural bentonite, Adsorption 13 (2007) 41–51, https://doi.org/10.1007/s10450-007-9003-y.
[36] T.S. Anirudhan, P.S. Suchithra, Equilibrium, kinetic and thermodynamic modeling for the adsorption of heavy metals onto chemically modified hydrotalcite, Indian J. Chem. Technol. 17 (2010) 247–259.
[37] B.S. Krishna, S. Selvaraj, B.V. Mohan, D.S.R. Murty, B.S. Jai Prakash, B.S. Krishna, B.S. Selvaraj, S. Mohan, B.V. Murty, D.S.R. Jai Prakash, Chemically modified clays as recyclable adsorbents for iodine, Bull. Mater. Sci. 21 (1998) 355–361, https://doi.org/10.1007/BF02744966.
[38] J. Bors, A. Gorny, S. Dultz, Sorption characteristics of radioiodide on organophilic bentonite, Radiochim. Acta 78 (1997) 117–121, https://doi.org/10.1524/ract.1997.78.special-issue.117.
[39] M.C. Pazos, M.A. Castro, A. Cota, F.J. Osuna, E. Pavón, M.D. Alba, New insights into surface-functionalized swelling high charged micas: their adsorption performance for non-ionic organic pollutants, J. Ind. Eng. Chem. 52 (2017) 179–186.
[40] S.M. Rao, S. Sivachidambaram, Characterization and iodide adsorption behaviour of HDPY+ modified bentonite, Environ. Earth Sci. 68 (2013) 559–566, https://doi.org/10.1007/s12665-012-1759-z.
[41] J. Bors, A. Gorny, S. Dultz, Some factors affecting the interactions of organophilic clay minerals with radioiodine, Radiochim. Acta 66–67 (2015) 309–314, https://doi.org/10.1524/ract.1994.6667.special-issue.309.
[42] B. Riebe, J. Bors, S. Dultz, Retardation capacity of organophilic bentonite for anionic fission products, J. Contam. Hydrol. 47 (2001) 255–264.
[43] B. Riebe, S. Dultz, C. Bunnenberg, Temperature effects on iodine adsorption on organo-clay minerals – I. Influence of pretreatment and absorption temperature, Appl. Clay Sci. 28 (2005) 9–16, https://doi.org/10.1016/j.clay.2004.01.004.
[44] A. Zhang, J. Xiang, L. Sun, S. Hu, P. Li, J. Shi, P. Fu, S. Su, Preparation, characterization, and application of modified chitosan sorbents for elemental mercury removal, Ind. Eng. Chem. Res. 48 (2009) 4980–4989, https://doi.org/10.1021/ie9000629.
[45] X.L. Zhou, F. Solymosi, P.M. Blass, K.C. Cannon, J.M. White, Interactions of methyl halides (Cl, Br and I) with Ag(111), Surf. Sci. 219 (1989) 294–316, https://doi.org/10.1016/0039-6028(89)90214-8.
[46] D.W. Smith, Ionic hydration enthalpies, J. Chem. Educ. 54 (1977) 540–542.
[47] C. Hinz, Description of sorption data with isotherm equations, Geoderma 99 (2001) 225–243.
[48] G. Limousin, J.P. Gaudet, L. Charlet, S. Szenknect, V. Barthès, M. Krimissa, Sorption isotherms: a review on physical bases, modeling and measurement, Appl. Geochem. 22 (2007) 249–275.
[49] E. Galunin, M.D. Alba, M.J. Santos, T. Abrão, M. Vidal, Lanthanide sorption on smectitic clays in presence of cement leachates, Geochim. Cosmochim. Acta 74 (2010) 862–875.
[50] Y. Park, W.S. Shin, S.J. Choi, Removal of Co, Sr and Cs from aqueous solution using self-assembled monolayers on mesoporous supports, Korean J. Chem. Eng. 29 (2012) 1556–1566, https://doi.org/10.1007/s11814-012-0035-y.
[51] S. Bilgiç, M. Şahin, The corrosion inhibition of austenitic chromium-nickel steel in H2SO4 by 2-butyn-1-ol, Mater. Chem. Phys. 70 (2001) 290–295, https://doi.org/10.1016/S0254-0584(00)00534-4.